Editors' Suggestion

Criticality of the viscous to inertial transition near jamming in non-Brownian suspensions

Nishanth Murugan [1], Donald Koch [1,2] and Sarah Hormozi [1,2]
[1] *Sibley School of Mechanical and Aerospace Engineering, Cornell University, Ithaca, New York 14853, USA*
[2] *Robert Frederick Smith School of Chemical and Biomolecular Engineering, Cornell University, Ithaca, New York 14853, USA*

(Received 25 June 2025; accepted 14 May 2026; published 15 July 2026)

Dense non-Brownian suspensions undergo a viscous to inertial transition with increasing shear rate ($\dot{\gamma}$), from a regime of constant viscosity at low shear rates to a regime where the viscosity varies linearly with the shear rate. The shear rate associated with this transition has been shown to vary dramatically between different experimental systems. Using the discrete element method, we show that in the regime where frictional contacts are absent, the characteristic shear rate for the transition to an inertial state is sensitive to the volume fraction (ϕ) of the suspension and exhibits a critical behavior at the jamming volume fraction (ϕ_m) for the system. By uncovering the presence of a microstructural length scale (L_c) that controls the emergence of inertial effects in the suspension, it is shown that the criticality emerges as a consequence of L_c diverging at jamming. We further show that in contrast to the conventional Stokes number $St = \rho\, d^2\dot{\gamma}/\eta_f$, the definition of a modified Stokes number $St_{\text{cluster}} = \rho L_c^2\dot{\gamma}/\eta_f$ correctly quantifies the inertial effects within the suspension and leads to a collapse of the rheological data.

DOI: 10.1103/dz98-r4dd

I. INTRODUCTION

With increasing shear rate the stress of a suspension of rigid solid non-Brownian particles displays a transition from a viscous regime of Newtonian rheology ($\propto \dot{\gamma}$) to an inertial regime characterized by Bagnoldian rheology ($\propto \dot{\gamma}^2$) [1]. The rheology of dense non-Brownian suspensions is central to the physics of various natural phenomena (mudslides, landslides, avalanches, etc.) and is of critical importance in the industrial processing of cement slurry, ceramic materials, etc. [2–4]. In this paper, we are interested in the viscous to inertial transition which occurs due to the increasing role played by particle inertia in facilitating the transfer of momentum within the suspension. This rheological transition can give rise to flow instabilities and change the shape of the wavefront of mudslides. Importantly, it can magnify the impact force when the front of a mudslide collides with a rigid structure [5,6]. The characteristic shear rate for this transition ($\dot{\gamma}_{v\to i}$) is found to vary sensitively between different suspension recipes in the literature and across different works without any consensus on the physical mechanism that triggers the transition.

In the viscous regime of constant viscosity at low shear rates, particle inertia has minimal influence on the dynamics of the system, with the particle contact forces being balanced by the hydrodynamic lubrication forces within the suspension. As a result, the stress in this regime scales linearly with the shear rate and is given by $\Sigma_V \sim \eta_V(\phi)\,\eta_f\,\dot{\gamma}$, where η_f is the viscosity of the solvent phase and $\eta_V(\phi)$ captures the dependence of the stress on the volume fraction of the suspension. In the inertial regime wherein interparticle contact or collisions between particles control the transfer of momentum, the stress scales as $\Sigma_I \sim \eta_I(\phi)\,\rho\, a^2\dot{\gamma}^2$. Here, ρ and a represent the density and average radius of a particle. Intuitively, one would expect the transition to occur when the viscous and inertial stresses are similar in magnitude. This results in the definition of a nondimensional Stokes number given by $St = 4\rho a^2\dot{\gamma} / \eta_f$, which is a measure of the relative strength of inertial and viscous stresses within the suspension at the particle scale. This leads one to predict the transition to occur at a characteristic Stokes number, $St_{v\to i} \approx 1$. However, experimental [7–11] and numerical [12–14] investigations into the viscous to inertial transition in dense suspensions have yielded varied results on $St_{v\to i}$.

Experiments presented in [7,8,10] are performed on a suspension of polystyrene spheres with radii of roughly $\sim$40− μm immersed in an aqueous solution. Atomic force microscopy (AFM) measurements on this sample [8,10] confirmed that electrostatic forces between the particles are sufficiently strong to render the suspension effectively frictionless across the experimentally measured stress range. In this system, the transition to inertial rheology occurs at shear rates lower than those associated with the frictionless to frictional discontinuous shear thickening (DST) transition [15], where stresses become large enough to overcome the repulsive barrier and activate frictional contacts. More interestingly, these experiments [7,8] show that $St_{v\to i}$ varies as a function of ϕ and goes to zero as the volume fraction approaches jamming. In contrast, the work of [9] uses a suspension made up of PMMA particles that are roughly $\sim$4.65 mm in size. This yields a frictional suspension because the length scale associated with colloidal forces is much smaller than the roughness of the particles so that particles come into physical contact during the suspension flow. The rheology of this system was shown to yield $St_{v\to i} \approx 10$, independent of the volume fraction of the suspension.

For the frictionless suspension, a theoretical approach using perturbation theory was made in [16] to rationalize the results of [7] indicating a varying $St_{v\to i}(\phi)$. It was argued that the dissipation of power injected into the system was dominant within isolated rivulets, where the relative velocity v_r between the particles was larger than the affine relative motion by a lever factor defined as $\mathcal{L} = v_r/2a\dot{\gamma}$. The dissipation in the viscous and inertial regimes was shown to scale as $\sim\mathcal{L}^2$ and $\sim\mathcal{L}^4$, respectively, resulting in a criticality $\dot{\gamma}_{v\to i} \sim \mathcal{L}^{-2} \sim (\phi_m - \phi)^{2.83}$. However, this scaling was based on an assumption that the lever effect acts on all neighboring particles in the system rather than representing the strong shearing motion occurring only in the isolated rivulets envisioned earlier in the argument proposed by [16]. This leads to a prediction for the vanishing shear rate of transition at jamming with an exponent $\sim$2.83, that is significantly different from the observation ($\sim$1) in [7].

Attempts made using numerical simulations on the viscous to inertial transition in frictional dense suspensions have shown the transition to be independent of ϕ but with widely different values, $St_{v\to i} \approx 1.5$ [12], $St_{v\to i} \approx 1$ [13], and $St_{v\to i} \approx 0.01$ [14], obtained by different investigators that are all different from the value inferred from experiments [9], $St_{v\to i} \approx 10$. These stark differences between different experiments and numerical simulations motivate the need to explore the differences within the microstructure formed in frictional and frictionless suspensions and understand the mechanism underlying the transition among different types of non-Brownian suspensions.

In this work, we use a discrete element method (DEM) to examine the rheology of a dense non-Brownian frictionless suspension over a wide range of shear rates and volume fractions. We will show that the characteristic Stokes number for the viscous to inertial transition $St_{v\to i}$ in a frictionless suspension goes to zero as a nearly linear function of the distance to the jamming volume fraction $(\phi_m - \phi)$. A scaling framework will be used to achieve a collapse of the rheological data and to extract the exponents characterizing the critical behavior of the transition. The collapse of the data will be used to hypothesize the existence of a growing length scale of the microstructure that diverges at jamming. A study of the system size dependence of the simulated stress will be used to verify the existence of the diverging length scale and its relation to the critical behavior of the transition.

II. NUMERICAL METHOD

The DEM solves Newton's equations of motion (1) for each particle within the suspension by computing its interaction with all other particles in the system. In a frictionless non-Brownian suspension, two types of forces primarily dictate the dynamics: (i) a hydrodynamic lubrication force $\mathcal{F}^L_{ij}$ caused by the flow within the gap between two particles due to their relative motion, and (ii) a repulsive force $\mathcal{F}^R_{ij}$ caused by an electrostatic interaction between two particles. Due to the absence of a frictional contact force, the interaction torque between two particles comes purely from the lubrication flow within the gap between two particles ($\mathcal{T}^L_{ij}$). The pairwise nature of these forces and torques simplifies the DEM as they only act between a particle and its nearest neighbors. The equations of motion are

$$m\frac{d\boldsymbol{u}_i}{dt} = \sum_{j=1}^{N_{n,i}} \left(\mathcal{F}^L_{ij} + \mathcal{F}^R_{ij}\right), \quad I\frac{d\boldsymbol{\omega}_i}{dt} = \sum_{j=1}^{N_{n,i}} \mathcal{T}^L_{ij}, \quad \frac{d\boldsymbol{x}_i}{dt} = \boldsymbol{u}_i. \tag{1}$$

where $\boldsymbol{x}_i$, $\boldsymbol{u}_i$, and $\boldsymbol{\omega}_i$ represent the position, velocity, and angular velocity of the ith particle within the system. The net force and torque on the ith particle is calculated by summing its force and torque contributions arising from interactions with all $N_{n,i}$ neighbors. In the frictionless suspensions used in experiments [7,8,10], there is an electrostatic repulsive force that works to prevent particles from coming into contact resulting in a finite surface separation $h_{\min}$. Owing to the expensive computational requirements associated with resolving the small Debye length scale ($\lambda \approx 2$ nm as found in [10]) for the electrostatic repulsion in a simulation with a large domain, the repulsive force between two particles is modeled as a Hookean spring, $\mathcal{F}^R_{ij} = \mathcal{K}\,\delta\,\boldsymbol{n}$. Here, $\mathcal{K}$ is the stiffness of the spring, $\boldsymbol{n}$ is a unit vector along the line connecting the centers of two contacting particles, and δ measures the strength of the repulsive force based on the surface separation $h = r_{ij} - a_i - a_j$,

$$\delta = \begin{cases} 0 & h > h_{\min}, \\ h_{\min} - h & h < h_{\min}. \end{cases} \tag{2}$$

Here, r_{ij} is the distance between the centers of particles i and j, with a_i and a_j being their respective radii. The Hookean spring activates when $h < h_{\min}$, where $h_{\min}$ models the separation at which the electrostatic repulsion balances the shear-induced normal force. By maintaining a constant value of $h_{\min}$ we avoid the shear thinning associated with soft repulsive forces [15,17,18]. The expressions for the lubrication forces $\mathcal{F}^L_{ij}$ and torques $\mathcal{T}^L_{ij}$, that contain contributions from the squeeze, shear, and pump modes can be found in Appendix A of the Supplemental Material [19]. These asymptotic expressions diverge when the surface separation between the particles (h) goes to zero as $\sim 1/h$ for the squeeze mode and $\sim \log(a/h)$ for the shear and pump modes. In the frictionless suspension, however, the electrostatic repulsive barrier prevents particle surfaces from approaching within distances smaller than $h_{\min}$. The actual surface separation between the particles is thus h, when $h > h_{\min}$ and $h_{\min}$ when $h < h_{\min}$. As a result, the normal lubrication force is set to zero and the tangential lubrication force is calculated assuming that the surface separation is $h_{\min}$ when $h < h_{\min}$.

The dynamics of the system governed by Eq. (1) is dictated by four parameters: the volume fraction ϕ, the Stokes number St, the nondimensional surface separation at which the electrostatic repulsive forces constrain normal motion between the particles given by $h^*_{\min} = h_{\min}/a$ and a nondimensional number $\Gamma = \mathcal{K} \,/\, 6\pi\eta_f a\dot{\gamma}$ [20] that characterizes the strength of the repulsive forces, with respect to the hydrodynamic lubrication forces. For the frictionless suspension of non-Brownian spheres, 40 μm in diameter, as used in [7,8,10], the length scale of the electrostatic repulsive force measured using AFM, $l_d \approx 10^{-4}a$ [10]. In this work, we fix the value of $h^*_{\min} = 10^{-4}$. It is essential to have $\Gamma \gg 1$ to impose a strong resistance to normal motion between particles when the surface separation falls below $h_{\min}$. In the simulations, we choose values of Γ to vary from 10^5–10^7 [21] ensuring that we are firmly within the regime wherein increasing the stiffness of the Hookean spring further has a negligible effect on the rheology of the suspension as shown in Appendix A of the Supplemental Material [19]. This allows us to explore the rheology of the suspension within the parameter space of (ϕ, St).

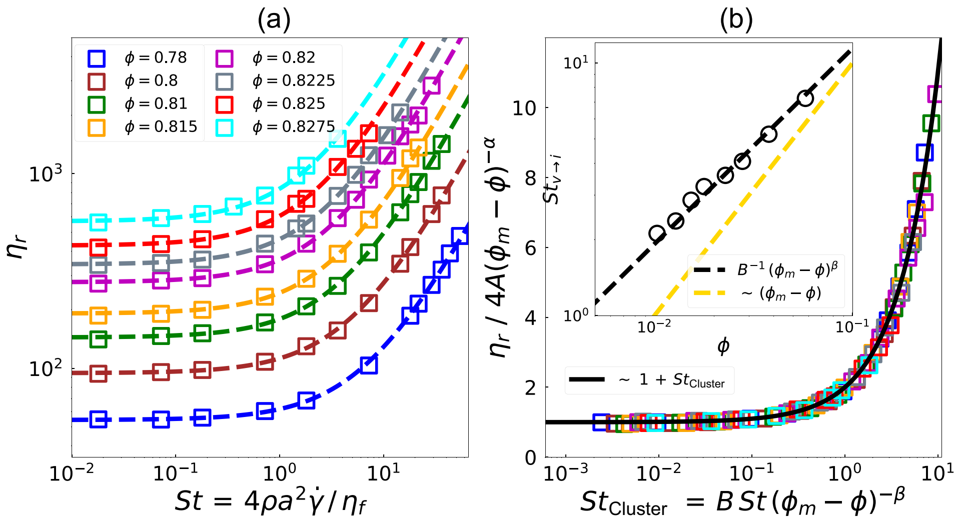

FIG. 1. Results from the 2D simulations. (a) Plot of the relative shear viscosity as a function of St for different volume fractions ϕ. The dashed lines depict the fitting function $\eta_r(St) = 4\,\mathcal{A}(\phi)\,(1 + \mathcal{B}(\phi)St)$ for each ϕ. (b) Collapse of the rheological data onto the solid black line $\sim 1 + St_{\text{cluster}}$, where $St_{\text{cluster}} = B\,St\,(\phi_m - \phi)^{-\beta} = \rho_p L_c^2\dot{\gamma}/\eta_f$ showcasing the accuracy of Eq. (3) fitted with parameters $\{A,\ B,\ \alpha,\ \beta,\ \phi_m\} = \{0.283,\ 0.015,\ 1.36,\ 0.774,\ 0.838\}$. In the inset, the circles correspond to $St_{v\to i}(\phi) = \mathcal{B}(\phi)^{-1}$. The dashed black line in the inset depicts the transition Stokes number obtained from Eq. (3), i.e., $B^{-1}(\phi_m - \phi)^{\beta}$. The dashed yellow line indicates linear scaling ($\beta = 1$) for comparison.

Within the framework of the DEM described thus far, we solve the equations of motion (1) for each particle within the system, with the simulation domain being subjected to Lees Edwards boundary conditions to generate a simple shear flow within a periodic domain. The particle polydispersity, defined as the ratio of the standard deviation to the mean of the particle size distribution, is fixed at 16% in the simulation to avoid the effects of crystallization. The simulations are performed in both 2D and 3D. In this work, the 2D simulations are run by initializing particles with the velocity along the vorticity direction and angular velocities in the flow-gradient plane to be zero. In addition, the force on the particles along the vorticity direction is set to zero when solving Eq. (1). This yields a two-dimensional shear flow of the suspension.

III. RESULTS

The simulation results for the macroscopic rheology of the 2D system at different volume fractions are displayed in Fig. 1(a). The curve for each value of ϕ demonstrates a regime of constant viscosity at low St, followed by a transition to a regime where the viscosity varies linearly with St. The dashed lines in the figure represent, $\eta_r(\phi, St) = 4\,\mathcal{A}(\phi)\,(1 + \mathcal{B}(\phi)St)$. The characteristic Stokes of transition $St_{v\to i}(\phi) = 1\,/\,\mathcal{B}(\phi)$, is marked by the viscous and inertial stresses being equal in magnitude and is plotted in the inset of Fig. 1(b). Interestingly, $St_{v\to i}$ appears to continuously decrease with ϕ and go to zero at jamming. To characterize the rheology across different ϕ and St, a scaling framework [Eq. (3)] is formulated. The divergence of the viscosity follows a power-law scaling of the distance to jamming, $(\phi_m - \phi)^{-\chi}$. The jamming volume fraction for a suspension is typically fixed by the particle size distribution and the interparticle friction coefficient associated with particle contacts. In the framework [Eq. (3)], ϕ_m is assumed to be the same in the viscous and inertial regimes, but the divergence is expected to have a different exponent χ (see Appendix B of the Supplemental Material [19] for a detailed explanation). Equation (3) is thus written as the sum

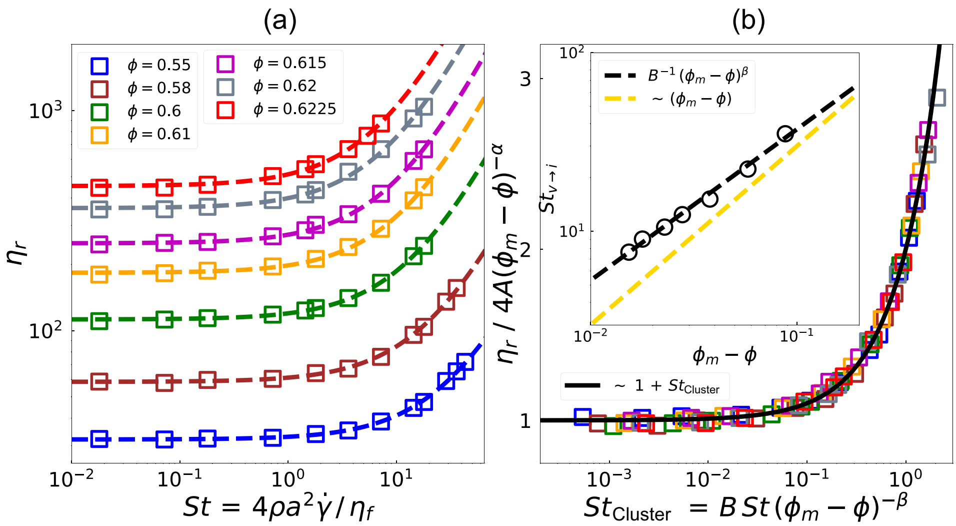

FIG. 2. Results from the 3D simulations. (a) Plot of the relative shear viscosity as a function of St for different volume fractions ϕ. The dashed lines depict the fitting function $\eta_r(St) = 4\mathcal{A}(\phi)(1 + \mathcal{B}(\phi)St)$ for each ϕ. (b) Collapse of the rheological data onto the solid black line $\sim 1 + St_{\mathrm{cluster}}$, where, $St_{\mathrm{cluster}} = B\,St\,(\phi_m - \phi)^{-\beta} = \rho_p L_c^2 \dot{\gamma}/\eta_f$ showcasing the accuracy of Eq. (3) fitted with parameters $\{A,\ B,\ \alpha,\ \beta,\ \phi_m\} = \{0.193,\ 0.004,\ 1.53,\ 0.845,\ 0.638\}$. In the inset, the circles correspond to $St_{v\to i}(\phi) = \mathcal{B}(\phi)^{-1}$. The dashed black line in the inset depicts the transition Stokes number obtained from Eq. (3), i.e., $B^{-1}(\phi_m - \phi)^{\beta}$. The dashed yellow line indicates linear scaling ($\beta = 1$) for comparison.

of two distinct power-law scalings of the distance to jamming,

$$\eta_r(\phi, St) = 4A(\phi_m - \phi)^{-\alpha}(1 + B\,St\,(\phi_m - \phi)^{-\beta}). \tag{3}$$

Consequently, the shear viscosity diverges as $\eta_r \sim (\phi_m - \phi)^{-\alpha}$ at low shear rates ($St \ll 1$) in the viscous regime, and with a different power law $\eta_r \sim (\phi_m - \phi)^{-(\alpha+\beta)}$ in the inertial regime at large shear rates ($St \gg 1$). The success of this framework in unifying the rheology across different ϕ and St is showcased in Fig. 1(b), wherein a rescaling yields a collapse of the rheological data for the viscous to inertial transition. A similar set of results is derived for the 3D simulations by applying the framework given by Eq. (3) and achieving a collapse of the data, as shown in Figs. 2(a) and 2(b), respectively. The scaling law also shows the critical behavior of the transition, wherein ($\dot{\gamma}_{v\to i}$) goes to zero as $\sim(\phi_m - \phi)^{\beta}$, with exponents $\beta = 0.77$ and 0.84 in 2D and 3D, respectively. These results indicate that a suspension at jamming displays an inertial scaling of the stress even at the smallest shear rates.

More importantly, the decrease in $St_{v\to i}$ as a function of ϕ calls into question, the accuracy of using a Stokes number defined based on the average particle size to quantify the role of inertia in the suspension behavior. It also hints at the existence of a microstructural length scale L_c, larger than the average particle size, with the criticality of $St_{v\to i}$ arising as a consequence of L_c diverging at jamming. This idea is further supported by the need for a modified Stokes number, $St_{\mathrm{cluster}} = B\,St\,(\phi_m - \phi)^{-\beta} = \rho_p L_c^2\dot{\gamma}/\eta_f$, in collapsing the data [Figs. 1(b) and 2(b)]. Hence, the length scale of the microstructure can be expected to diverge as $L_c \sim (\phi_m - \phi)^{-\beta/2}$, with $\beta/2 \approx 0.4$.

The idea of a diverging length scale of the microstructure at jamming has been proposed in previous works using arguments built from velocity correlation functions [22], finite-size scaling analysis [23], and scaling arguments derived by perturbing a jammed state [16,24,25]. In [24,25], the decay of an applied perturbation (removing a single contact) to a jammed state was used to extract a length scale l_c, which was shown to scale with the distance from isostaticity as $l_c \sim 1/\sqrt{\delta z}$. Here,

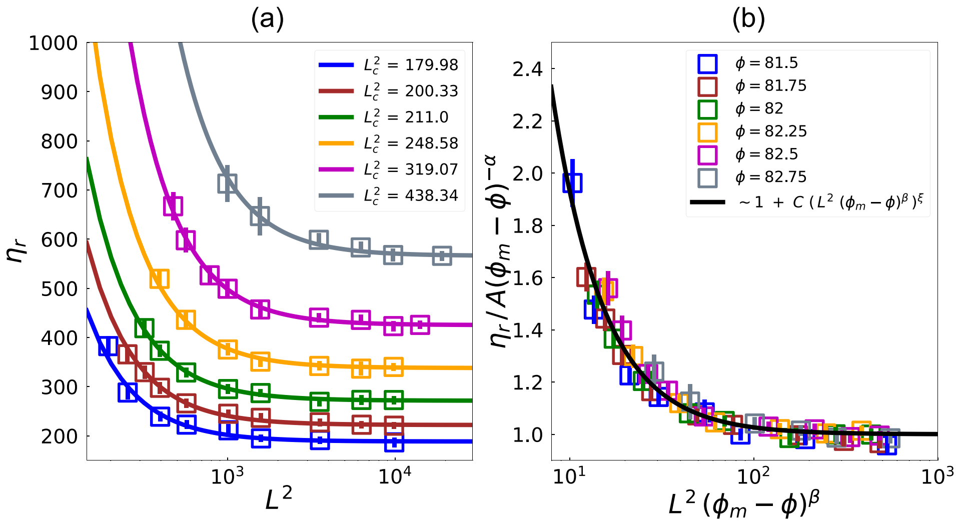

FIG. 3. The results for the system size dependence in the 2D simulations at $St = 0.018$. (a) The points depict the shear viscosity as a function of the box size. The solid lines depict the fit $\eta_r(\phi, L^2) = \mathcal{R}(\phi)$ $(1 + (L^2 / L_c^2)^\xi)$. (b) A collapse of the points from Fig. 3(a) is achieved by rescaling η_r and L^2. The solid black line represents the comprehensive fit [Eq. (4)] with $\xi = 1.54$ and $C = 32.66$.

$\delta z = z_c - z$, with z being the coordination number. A later work [16], argued that a perturbation applied to such a jammed state creates a stress anisotropy $\delta\mu$, where μ is the ratio of the shear stress to the pressure, that scales as $\delta\mu \sim \delta z^{0.35}$ and is related to the opening of the weakest contact. It was then proposed that the opening of a contact triggers an avalanche that perturbs the overall volume fraction resulting in $\delta\mu \sim \delta\phi$. These arguments were combined to predict the divergence of a length scale associated with the microstructure, $l_c \sim (\phi_m - \phi)^{-0.43}$, close to jamming. This prediction of the exponent associated with the divergence of l_c put forth in [16,25] is quite close to the result inferred from the rheological results discussed in Figs. 1 and 2.

To show the presence of the microstructural length scale within the suspension and its role in triggering the transition, a series of tests are performed to probe the system size dependence of the rheology at different values of ϕ. The results of these tests for the 2D [Fig. 3(a)] and 3D [Fig. 4(a)] simulations show that there is an increase in the viscosity with decreasing size of the periodic cell. Here, L represents the length of the square and cubic simulation box in 2D and 3D, respectively. As we decrease the box size L, at a critical size of the box L_c, the cluster spans the whole domain. A further decrease of the box size $L < L_c$ results in an increased viscosity due to a collision of the cluster with itself by reaching through the periodic boundary. It should be noted that the results in Figs. 1 and 2 were obtained using a domain size $L \gg L_c$, ensuring that the reported rheology and scaling laws are free from finite-size effects.

The results from the system size dependence are fit using the function, $\eta_r(\phi, L^2) = \mathcal{R}(\phi)$ $(1 + (L^2 / L_c^2)^\xi)$, to extract an approximate length scale for the cluster $L_c(\phi)$. From the results on the rheology given in Figs. 1 and 2, we expect the size of the cluster L_c to scale as $L_c^2 \sim (\phi_m - \phi)^{-\beta}$ with the appropriate value of β corresponding to the 2D and 3D simulations. Here, $\mathcal{R}(\phi)$ depicts the system size independent rheology ($L \gg L_c$). The estimated value of L_c differs between the 2D and 3D simulations [Figs. 3(a) and 4(a)]. We attribute this to the geometric constraint in 2D, where the cluster is restricted to remain entirely within the flow-gradient plane. In 3D, by contrast, the cluster can rotate partially into the vorticity direction, even though its formation is still biased toward the flow-gradient plane. This additional degree of freedom may also explain the difference in $St_{v\to i}$ observed between the 2D and 3D simulations [see Figs. 1(b) and 2(b)].

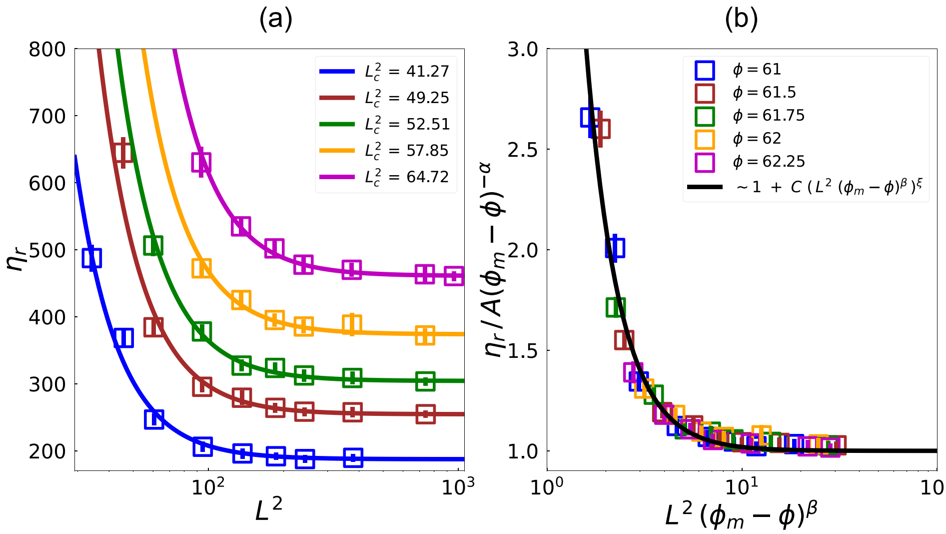

FIG. 4. The results for the system size dependence in the 3D simulations at $St = 0.18$. (a) The points depict the shear viscosity as a function of the box size. The solid lines depict the fit $\eta_r(\phi, L^2) = \mathcal{R}(\phi)(1 + (L^2/L_c^2)^\xi)$. (b) A collapse of the points from Fig. 3(a) is achieved by rescaling η_r and L^2. The solid black line represents the comprehensive fit [Eq. (4)] with $\xi = 2.53$ and $C = 6.43$.

For the results shown in Figs. 3(a) and 4(a) which correspond to the viscous regime, the fitting simplifies as

$$\eta_r(\phi, L^2) = A(\phi_m - \phi)^{-\alpha}[1 + C(L^2(\phi_m - \phi)^\beta)^\xi]. \tag{4}$$

Rescaling η_r and L^2 using the values of A, ϕ_m, α, and β known from previous results, it is possible to collapse the data in Fig. 3(a) into a single curve as shown in Fig. 3(b) by fitting parameters C and ξ. A similar exercise is repeated for the 3D results as shown in Fig. 4. The observed collapse of the results for the system size dependence of the rheology, by applying the scaling for the cluster size $L_c \sim (\phi_m - \phi)^{-\beta/2}$, determined from the results on the viscous to inertial transition (Figs. 1 and 2), verifies the existence of an extended suspension microstructure that governs the transition.

IV. DISCUSSION

In summary, using DEM simulations we have shown that the transition from a viscous regime to an inertial regime in a dense non-Brownian frictionless suspension displays a critical behavior close to jamming, $St_{v\to i} \sim (\phi_m - \phi)^\beta$. The values for the exponent $\beta = 0.77$ and 0.85 obtained from the 2D and 3D simulations are in close alignment with the experimentally observed results of $St_{v\to i} \sim (\phi_m - \phi)^1$ [7]. This stands in marked contrast to the framework of [16], which attributes the transition to a change in the balance of energy dissipation mechanisms and predicts $\dot{\gamma}_{v\to i} \sim (\phi_m - \phi)^{2.83}$. Such a steep divergence has not been observed in either simulations or experiments. Instead, our results point to a different physical origin wherein the criticality of $St_{v\to i}$ emerges from a growing microstructural length scale that diverges at jamming, $L_c \sim (\phi_m - \phi)^{-\beta/2}$. This mechanism not only rationalizes the observed scaling but also naturally explains why the use of modified Stokes number St_{cluster} based on L_c collapses the rheological data across both regimes.

Our findings reveal a fundamental relationship between the cluster size and the macroscopic properties of the suspension, wherein the transfer of momentum over a length scale much larger than the size of a single particle leads to the suspension becoming inertial at a lower shear rate. The existence of a cluster within the suspension strongly highlights the nonlocal rheology of the system.

This motivates the need for a nonlocal theory [26,27], as the stress within the cluster is affected by the forces it experiences over its entire length, thus requiring a framework that captures how stress is transmitted through the suspension during cluster formation, breakup, and interactions with other particles. It is also pertinent to note that experimental investigations on a frictional suspension of particles [9] have shown a constant $St_{v \to i}$ with increasing ϕ. This raises a question whether a diverging microstructural length scale also occurs near jamming for frictional suspensions. It would be surprising for there to be constant $St_{v \to i}$ in the presence of a diverging microstructural length scale. Future studies on the scaling for the cluster size close to jamming in frictional suspensions and its role in triggering the transition are necessary to establish a unified theory across different flowing regimes.

ACKNOWLEDGMENT

This work was supported by the NSF Grants No. CBET-1554044 and No. CBET-2210322. The authors report no conflict of interest.

DATA AVAILABILITY

There are no publicly available research data or software supporting this manuscript. Requests for further information or data should be sent to the authors.

[1] R. A. Bagnold, Experiments on a gravity-free dispersion of large solid spheres in a Newtonian fluid under shear, Proc. R. Soc. London A **225**, 49 (1954).

[2] J. J. Stickel and R. L. Powell, Fluid mechanics and rheology of dense suspensions, Annu. Rev. Fluid Mech. **37**, 129 (2005).

[3] É. Guazzelli and O. Pouliquen, Rheology of dense granular suspensions, J. Fluid Mech. **852**, P1 (2018).

[4] C. Ness, R. Seto, and R. Mari, The physics of dense suspensions, Annu. Rev. Condens. Matter Phys. **13**, 97 (2022).

[5] N. J. Balmforth and A. Provenzale, *Geomorphological Fluid Mechanics* (Springer, Berlin, 2008), Vol. 582.

[6] P. Coussot, *Mudflow Rheology and Dynamics* (Routledge, Oxfordshire, UK, 2017).

[7] A. Fall, A. Lemaitre, F. Bertrand, D. Bonn, and G. Ovarlez, Shear thickening and migration in granular suspensions, Phys. Rev. Lett. **105**, 268303 (2010).

[8] Y. Madraki, A. Oakley, A. Nguyen Le, A. Colin, G. Ovarlez, and S. Hormozi, Shear thickening in dense non-Brownian suspensions: Viscous to inertial transition, J. Rheol. **64**, 227 (2020).

[9] F. Tapia, M. Ichihara, O. Pouliquen, and É. Guazzelli, Viscous to inertial transition in dense granular suspension, Phys. Rev. Lett. **129**, 078001 (2022).

[10] A. V. N. Le, A. Izzet, G. Ovarlez, and A. Colin, Solvents govern rheology and jamming of polymeric bead suspensions, J. Colloid Interface Sci. **629**, 438 (2023).

[11] F. Tapia, C.-W. Hong, P. Aussillous, and É. Guazzelli, Rheology of suspensions of non-Brownian soft spheres across the jamming and viscous-to-inertial transitions, Phys. Rev. Lett. **133**, 088201 (2024).

[12] M. Trulsson, B. Andreotti, and P. Claudin, Transition from the viscous to inertial regime in dense suspensions, Phys. Rev. Lett. **109**, 118305 (2012).

[13] C. Ness and J. Sun, Shear thickening regimes of dense non-Brownian suspensions, Soft Matter **12**, 914 (2016).

[14] T. T. Vo, S. Nezamabadi, P. Mutabaruka, J.-Y. Delenne, and F. Radjai, Additive rheology of complex granular flows, Nat. Commun. **11**, 1476 (2020).

[15] R. Mari, R. Seto, J. F. Morris, and M. M. Denn, Shear thickening, frictionless and frictional rheologies in non-Brownian suspensions, J. Rheol. **58**, 1693 (2014).

[16] E. DeGiuli, G. Düring, E. Lerner, and M. Wyart, Unified theory of inertial granular flows and non-Brownian suspensions, Phys. Rev. E **91**, 062206 (2015).
[17] I. M. Krieger, Rheology of monodisperse latices, Adv. Colloid Interface Sci. **3**, 111 (1972).
[18] B. J. Maranzano and N. J. Wagner, The effects of interparticle interactions and particle size on reversible shear thickening: Hard-sphere colloidal dispersions, J. Rheol. **45**, 1205 (2001).
[19] See Supplemental Material at http://link.aps.org/supplemental/10.1103/dz98-r4dd for a description of the discrete element method (DEM) used in the simulations (Appendix A) and a detailed discussion of jamming in the viscous and inertial regimes (Appendix B), which includes Refs. [7,8,10,28].
[20] S. Gallier, E. Lemaire, F. Peters, and L. Lobry, Rheology of sheared suspensions of rough frictional particles, J. Fluid Mech. **757**, 514 (2014).
[21] A. Goyal, N. S. Martys, and E. Del Gado, Flow induced rigidity percolation in shear thickening suspensions, J. Rheol. **68**, 219 (2024).
[22] P. Olsson and S. Teitel, Critical scaling of shear viscosity at the jamming transition, Phys. Rev. Lett. **99**, 178001 (2007).
[23] T. Kawasaki, D. Coslovich, A. Ikeda, and L. Berthier, Diverging viscosity and soft granular rheology in non-Brownian suspensions, Phys. Rev. E **91**, 012203 (2015).
[24] G. Düring, E. Lerner, and M. Wyart, Phonon gap and localization lengths in floppy materials, Soft Matter **9**, 146 (2013).
[25] G. Düring, E. Lerner, and M. Wyart, Length scales and self-organization in dense suspension flows, Phys. Rev. E **89**, 022305 (2014).
[26] R. L. Schiek and E. S. Shaqfeh, A nonlocal theory for stress in bound, Brownian suspensions of slender, rigid fibres, J. Fluid Mech. **296**, 271 (1995).
[27] E. S. Shaqfeh and G. H. Fredrickson, The hydrodynamic stress in a suspension of rods, Phys. Fluids **2**, 7 (1990).
[28] T. Schwager and T. Pöschel, Coefficient of restitution and linear-dashpot model revisited, Granular Matter **9**, 465 (2007).